Journal of Magnetic Resonance 288 (2018) 11–22

Contents lists available at ScienceDirect

Journal of Magnetic Resonance

journal homepage: www.elsevier.com/locate/jmr

X-band EPR setup with THz light excitation of Novosibirsk Free Electron Laser: Goals, means, useful extras

Sergey L. Veber [a,b,*], Sergey V. Tumanov [a,b], Elena Yu. Fursova [a], Oleg A. Shevchenko [c], Yaroslav V. Getmanov [c], Mikhail A. Scheglov [c], Vitaly V. Kubarev [b,c], Daria A. Shevchenko [c], Iaroslav I. Gorbachev [c], Tatiana V. Salikova [c], Gennady N. Kulipanov [c], Victor I. Ovcharenko [a], Matvey V. Fedin [a,b]

[a] International Tomography Center, SB RAS, Novosibirsk 630090, Russia
[b] Novosibirsk State University, Novosibirsk 630090, Russia
[c] Budker Institute of Nuclear Physics, SB RAS, Novosibirsk 630090, Russia

ARTICLE INFO

Article history:
Received 6 October 2017
Revised 10 January 2018
Accepted 11 January 2018
Available online 12 January 2018

Keywords:
Electron paramagnetic resonance
Free electron laser
NovoFEL
THz radiation
T-jump EPR

ABSTRACT

Electron Paramagnetic Resonance (EPR) station at the Novosibirsk Free Electron Laser (NovoFEL) user facility is described. It is based on X-band (~9 GHz) EPR spectrometer and operates in both Continuous Wave (CW) and Time-Resolved (TR) modes, each allowing detection of either direct or indirect influence of high-power NovoFEL light (THz and mid-IR) on the spin system under study. The optics components including two parabolic mirrors, shutters, optical chopper and multimodal waveguide allow the light of NovoFEL to be directly fed into the EPR resonator. Characteristics of the NovoFEL radiation, the transmission and polarization-retaining properties of the waveguide used in EPR experiments are presented. The types of proposed experiments accessible using this setup are sketched. In most practical cases the high-power radiation applied to the sample induces its rapid temperature increase (T-jump), which is best visible in TR mode. Although such influence is a by-product of THz radiation, this thermal effect is controllable and can deliberately be used to induce and measure transient signals of arbitrary samples. The advantage of tunable THz radiation is the absence of photo-induced processes in the sample and its high penetration ability, allowing fast heating of a large portion of virtually any sample and inducing intense transients. Such T-jump TR EPR spectroscopy with THz pulses has been previewed for the two test samples, being a useful supplement for the main goals of the created setup.

1. Introduction

THz (far-IR) range of electromagnetic radiation is being intensively explored nowadays, with many rich scientific opportunities still not implemented [1]. The main reasons limiting the progress in THz science and technology are the lack of intense THz sources and sensitive THz detectors [2]. Among the variety of the developed THz sources [3], only free electron based ones, in general, provide such unique properties of THz radiation as tunability and high power [4]. In addition, Free Electron Lasers (FELs) feature coherent light and picosecond-pulse time structure [5], making them sources of choice for fundamental and applied research.

Extreme high-field/high-frequency Electron Paramagnetic Resonance (EPR) spectroscopy operates in (sub-)THz range and follows the instrumentation progress in this field [6]. In the "high-field" direction the boundaries are almost identified. The world record constant field of 45 T was achieved for hybrid magnet [7,8], and a 25 T resistive magnet with high homogeneity (up to 1 ppm over a sphere of 1 cm with shimming) [9] is being used for EPR studies (ν_{mw} is up to 700 GHz for $g = 2$ systems) demonstrating the advantages of superior spectral resolution [10,11]. The use of superconducting magnets in EPR spectroscopy is more convenient for routine studies; however, the magnetic field strength in such systems reported in literature is currently limited by ~17 T [12]. Implementation of the pulsed magnets allows one to increase the accessible maximum magnetic field up to 100 T [13–16]. At these fields the electron Larmor frequency reaches almost 3 THz stressing the crucial importance of THz sources for extreme high-field/high-frequency EPR.

* Corresponding author at: International Tomography Center, SB RAS, Novosibirsk 630090, Russia.
E-mail address: sergey.veber@tomo.nsc.ru (S.L. Veber).

https://doi.org/10.1016/j.jmr.2018.01.009
1090-7807/

The majority of high-field/high-frequency EPR spectrometers based on solid-state harmonic oscillators operates at microwave (mw) frequencies up to 500 GHz [17–30] and mainly focuses on chemical and biological applications which strongly benefit from the high spectral resolution. The spectrometers operating at even higher frequencies (up to 3 THz) are based on the backward-wave oscillators [12,31,32], gyrotron [33] and CO_2 laser systems with different lasing gases [15,34–37]. The use of very-high-frequency sources is especially meaningful when studying the high-spin systems $S \geq 1$ with the zero-field splitting (ZFS) up to tens of cm^{-1}. For measurements of very large ZFS (up to a few hundreds of cm^{-1}) typical for some of the transition-metal ions, another approach called frequency-domain Fourier-transform THz-EPR (FD-FT THz-EPR) can be used [38–40]. Broadband radiation source such as mercury lamp or synchrotron is used in FD-FT THz-EPR experiments. The use of narrow band high-power FEL radiation grants unique opportunities for EPR spectroscopy, such as 6 ns length of $\pi/2$ pulses at 240 GHz [41] and frequency range of 1.2–75 THz combined with pulsed magnetic fields up to 70 T [42]. A considerable coherence of the individual THz micropulses of the FEL was demonstrated for narrow EPR lines [43], which is a prerequisite for a resonant control and THz electron spin echo spectroscopy.

Taking into account that the frequency range accessible by Novosibirsk FEL (NovoFEL) starts from ~1.2 THz and expands up to mid-IR range (~30 THz), we have chosen different experimental concept of EPR setup based on NovoFEL. We do not aim at EPR detection with THz frequency, but we use conventional X-band (~9 GHz) EPR for observation of direct/indirect influence of high-power NovoFEL light on the spin system under the study (such experiments can be called "THz-pump – EPR-probe"). In the following sections we discuss the main goals of the project and describe this X-band Continuous Wave (CW) and Time-Resolved (TR) EPR setup with THz light excitation fed from NovoFEL. We briefly introduce the design and some parameters of NovoFEL important for the proposed EPR experiments. We describe optical system allowing NovoFEL radiation to be fed into the EPR probehead, as well as the transmission and polarization-retaining properties of the waveguide used in our experiments. Possible experimental techniques utilizing the time profile of the NovoFEL radiation and CW/TR EPR are discussed. It is shown that the interaction of high-power THz light with the sample leads to its rapid heating, giving rise to intense T-jump induced transient EPR signals at low temperatures. Thermal dynamics of typical EPR samples is measured, and possible use of these extra effects is discussed.

2. Objectives

The studies in field of molecular magnetism pay significant attention to the high-spin systems with large ZFS as promising candidates for ultradense magnetic memory units [44,45] and quantum computing elements [46,47]. As was mentioned in Introduction, most of the single-high-frequency EPR spectrometers operate in a frequency range of 0.5–1 THz and magnetic fields up to 17 T; therefore they have strict limitations of the magnitudes of ZFS attainable for investigation [6]. In turn, FD-FT THz-EPR spectroscopy expands the mw frequency range up to several THz granting the precise determination of very large ZFS (~100 cm^{-1} and higher). Well-defined parameters of high-spin system allow selective excitation of its spin levels. This opens up a perspective, e.g., to study the relaxation times of the excited spin levels and to manipulate the magnetization of paramagnetic species. The excitation of spin levels by mw pulse of Gunn oscillator ($\nu_{mw} \sim 110$ GHz, $P_{mw} \sim 30$ mW) has been successfully used previously to study the magnetization dynamics in single-molecule magnet (SMM) Fe_8 [48]. However, if the splitting of spin energy levels exceeds the above-mentioned sub-THz values, perhaps only FELs can grant THz power and frequency tunability required for such experiments.

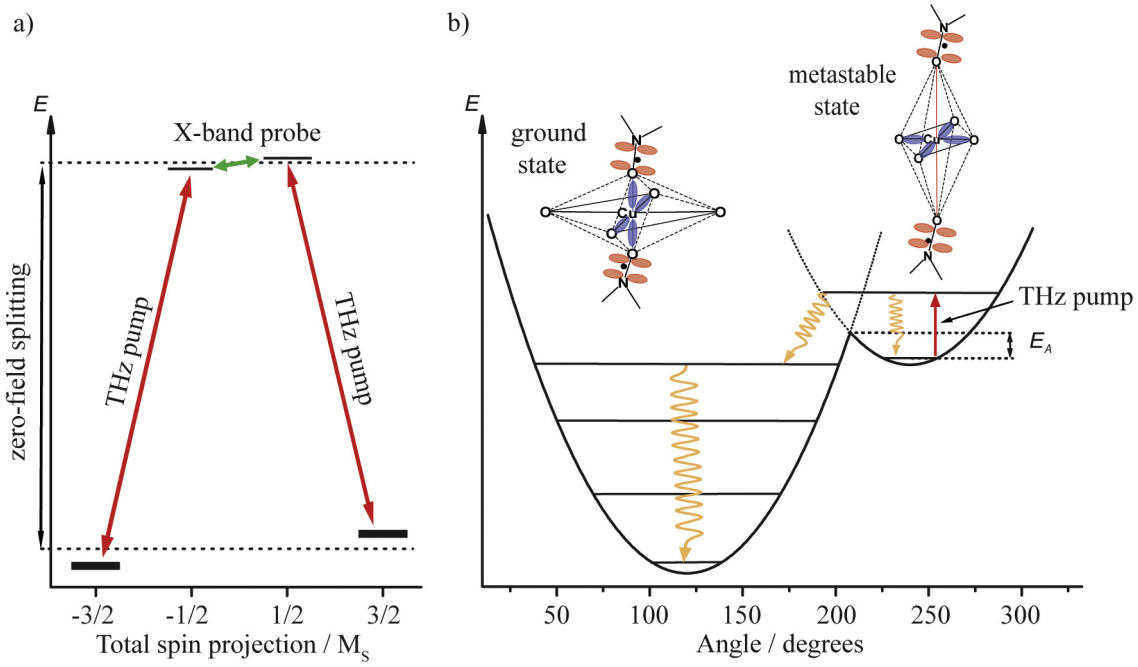

Fig. 1. (a) Energy levels of S = 3/2 spin system with negative axial ZFS parameter in the external magnetic field. Red arrows show EPR transitions which can be induced by THz light. X-band accessible EPR transitions are shown by green arrow. (b) Schematic circular section of the potential energy surface associated with the two Jahn–Teller valleys in nitroxide-copper(II)-nitroxide three-spin cluster. Structures corresponding to ground and metastable geometries are sketched on top; spin density of copper(II) ion and nitroxide radicals is depicted. Expected mechanism of the reverse conversion induced by THz radiation is shown. (For interpretation of the references to colour in this figure legend, the reader is referred to the web version of this article.)

With respect to SMMs, the objective of X-band EPR setup at NovoFEL is to develop the approach for manipulation of SMM magnetization, where we currently consider single-ion magnets (SIMs) based on the high-spin cobalt(II) as most suitable (spin system S = 3/2). General idea of the proposed experiments is sketched in Fig. 1a: resonant pumping of the spin transitions between ±1/2 and ±3/2 Kramers doublets should induce detectable changes in the X-band EPR spectrum of studied compound. Such changes are expected to be most pronounced for the spin 3/2 system characterized by axial ZFS tensor with large negative D parameter (depicted in Fig. 1a). The compound is "EPR silent" at helium temperatures due to the thermal depletion of ±1/2 Kramers doublet [49]; however, resonant THz pumping of $-3/2 \leftrightarrow -1/2$ and/or $3/2 \leftrightarrow 1/2$ transitions should lead to the onset of X-band EPR spectra. Implementation of time-resolved EPR provides means to study the THz-induced spin dynamics on the timescale of tens ns. Moreover, high-spin systems with positive axial ZFS parameter D are also suitable for such investigations: THz pumping of $-1/2 \leftrightarrow -3/2$ and $1/2 \leftrightarrow 3/2$ transitions should result in partial depopulation of the ±1/2 ground levels leading to a suppression of the detected EPR signal.

Another objective of the X-band EPR setup at NovoFEL is also related to the field of molecular magnetism, in this case focusing on the magnetoactive compounds exhibiting magnetostructural bistability. Perhaps the brightest representatives of such complexes are Fe-based spin-crossover compounds [50]. The other interesting bistable compounds intensively studied by us using EPR are the copper(II) complexes with stable nitroxide radicals [51,52]. In particular, EPR has been demonstrated as a very informative technique to study both temperature- and light-induced transitions in such complexes [53–56]. At helium temperatures such complexes can be found either in ground or in metastable magnetostructural state (Fig. 1b). The lifetime of metastable state exceeds several days at 5 K for some of the complexes [57], but shortens abruptly due to relatively small activation energy barrier ($E_A \sim 10$–20 K) when the sample is warmed up to 15–20 K [55]. Taking into account E_A values, the relaxation process from the metastable to the ground state can be induced by the quanta of relatively small energy (compared to visible light) via excitation of the vibrational levels [58] (this mechanism is depicted in Fig. 1b) or low-energy *d-d* transitions of copper(II) ion [59]. In both cases the high-power NovoFEL radiation is perfectly suitable for such experiments.

Obviously, the discussed objectives do not cover all possible applications of the setup in the future, and we expect their number to increase in time. However, all conceivable experiments must at the first place carefully consider the concomitant heating effects being the inevitable consequence of the interaction of high-power THz light with the sample. The understanding of such heat-induced EPR effects is crucial for subsequent interpretations, and as such, these phenomena will be addressed in detail in the following sections of this work. Note also, that the samples which we selected for benchmarking the thermal heating effects are directly related to the main objectives of NovoFEL EPR station: they are the cobalt(II) complex and bistable copper(II)-nitroxide compound; therefore the test studies described below provide necessary grounds for the future implementation of the target experiments sketched in Fig. 1.

3. Design of setup and experiments

3.1. X-band EPR spectrometer

X-band (~9 GHz) EPR spectrometer combined with NovoFEL is based on modified commercial X-band mw bridge ER 046MRPTW (Bruker, Germany). Mw pulsing circuit similar to that described elsewhere [60] introduced into the original bridge. It was used for determination of the upper (~1.1 MHz) and lower (~1.1 Hz) frequency limits of the EPR detection scheme showing the frequency range accessible in TR mode (see Fig. S1 in Supplementary Material). In the EPR experiments performed with NovoFEL radiation the mw pulsing circuit was not used. Mw frequency was controlled by the Agilent 53131A-124 (Agilent, USA) frequency counter. EPR spectrometer is equipped with the Oxford Instruments temperature control system based on ER-4118CF cryostat and ITC503 (Oxford Instruments, UK) temperature controller, which allows us to perform the EPR experiments in the temperature range of 4–300 K. ER 4118X-MD5 resonator (Bruker, Germany) was used, but the dielectric sapphire insert was replaced by the bismuth germanate (BGO) one (4 mm inner diameter) to improve the quality of baseline in CW experiments [61]. Permalloy based electromagnet of 3 Ohm resistance was used to produce the magnetic field of up to 0.9 T (see Fig. S2 in Supplementary Material). The power supply SPS 40A-160V (ELIP, Russia) and Hall effect field controller BH 15 (Bruker, Germany) were used to control the magnetic field. The phase-sensitive detection of the EPR signal in CW mode was done using SR830 lock-in amplifier (Stanford Research Systems, USA). The G3-112/1 amplifier was used to amplify 100 kHz modulation sine wave of the SR830 that was applied to modulation coils of the EPR resonator. The maximum available modulation amplitude was 4 Gs; however, 2 Gs modulation was sufficient for the experiments described in this work. The detection of the EPR signals locked to the repetition rate of NovoFEL micropulses (3.7–7.5 MHz) can be done with 200 MHz lock-in amplifier SR844 (Stanford Research Systems, USA). Recording of the transient signals in TR mode was performed with LeCroy 9350AM oscilloscope (Teledyne Technologies, USA). fsc2 program running under GNU/Linux was used for controlling the spectrometer (web page: www.fsc2.org). Photograph of the EPR spectrometer combined with NovoFEL is shown in Fig. S3 of Supplementary Material.

3.2. Radiation source NovoFEL

The NovoFEL facility consists of three FELs. The main blocks of NovoFEL and their spacial layout are illustrated in Fig. S4 of Supplementary Material. A simplified scheme of NovoFEL is shown in Fig. 2. All the FELs use the electron beam of the same electron accelerator, a multi-turn energy recovery linac (ERL). Starting from low energy injector, electrons pass from one to four times

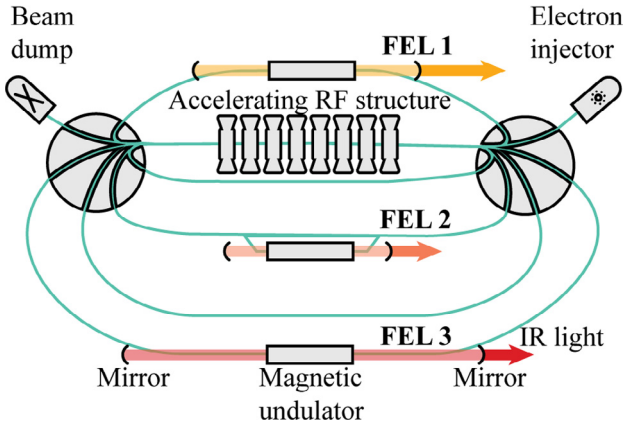

Fig. 2. Schematic view of the NovoFEL consisting of three FELs in its multi-turn ERL structure. Injector, linac, bending magnets, undulators, mirrors and dump are shown.

Table 1
Electron beam and radiation parameters of NovoFEL. Brief description of the parameters shown: 1 – the energy of electron in the beam in front of undulator; 2 – the electron current in the beam; 3 – the time between electron pulses (and radiation pulses) within continuous train; 4 – the duration of radiation pulse; 5 – the FWHM diameter of NovoFEL radiation beam at the output of nitrogen-filled beamline at EPR station; 6 – the maximum average radiation power.

FEL number	FEL1	FEL2	FEL3 rated	FEL3 achieved
Electron energy[1], MeV	12	22	46	42
Electron current[2], mA	30	10	50	3
Pulse repetition time[3], ns	180	133	267	267
Min. pulse duration[4], ps	70	20–50	10–20	10–20
Radiation linewidth (FWHM), %	0.2–1	0.2–1	0.1–1	0.1–1
Wavelength, μm	90–240	35–90	5–15	8.5–9.6
Wavenumber, cm^{-1}	110–40	285–110	2000–670	1170–1040
Radiation beam diameter[5], mm	35–50	15–25	5–18	8
Radiation power[6], kW	0.5	0.5	5	0.05

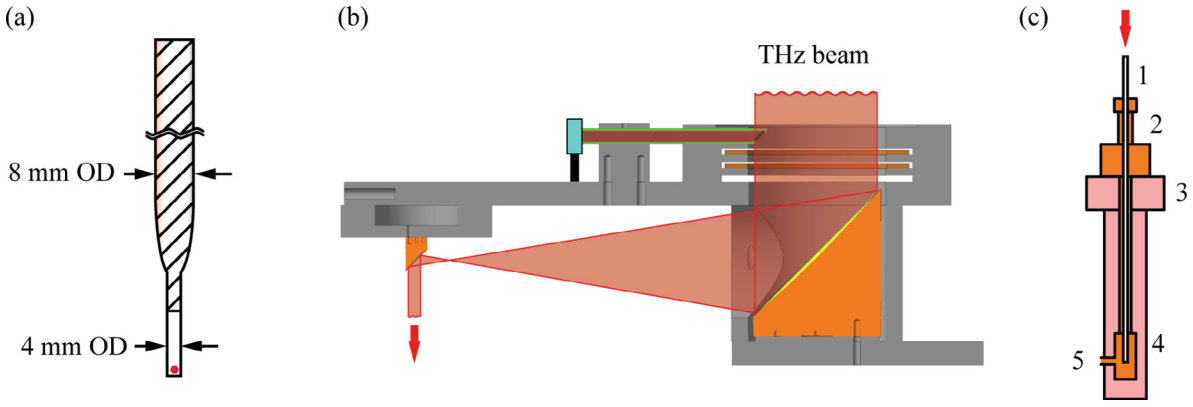

Fig. 3. (a) Sketch of the sample holder used for THz irradiation. Grid lines show silver mirror coating, red circle illustrates the sample. (b) Optical system based on two off-axis parabolic mirrors. THz beam path (red), parabolic mirrors (yellow), THz power probe (green) and power meter (cyan) are shown. (c) Irradiation scheme of the experiment. All parts of the EPR spectrometer except for cryostat and resonator are omitted. 1 – sample holder, 2 - EPR probehead, 3 – EPR cryostat, 4 – sample inside the EPR resonator, 5 – optical window of the cryostat. (For interpretation of the references to colour in this figure legend, the reader is referred to the web version of this article.)

(depending on the FEL used) through accelerating radio frequency (RF) structure. After that, they lose part of their energy ($\sim 10^{-3}$) in the FEL radiated system (undulator and optical resonator). The used electron beam is decelerated in the same RF structure, and the low-energy electrons are absorbed in the beam dump.

The radiation of all three FELs is released through opening in mirrors of the optical resonators, then it passes through the CVD-diamond windows, is directed to the radiation combiner and finally transferred through the nitrogen-filled beamline to the users stations [62]. The first FEL has been in operation since 2003 [63]. It provides a narrow-band (less than 1%) terahertz radiation in the wavelength range of 90–240 μm (Table 1) at an average power of up to 0.5 kW and a peak power of up to 1 MW (~100 ps pulses at a repetition rate of 5.6 MHz). The second FEL was commissioned in 2009 [64], it is based on two track ERL and works in far infrared spectral range (35–90 μm). The third FEL was commissioned in 2015 [65], it is based on four track ERL and the expected spectral range is 5–15 μm (mid infrared). Customization of the third FEL is in progress; average radiation power of 50 W was already achieved for the wavelength range of 8.5–9.6 μm.

NovoFEL is capable of producing up to 1 MW peak power in THz range, and owing to its recuperation scheme it is the most powerful source of THz coherent radiation in the world. NovoFEL radiation consists of continuous train of ~10–70 ps pulses with a repetition time from 133 to 267 ns (depending on the FEL used, Table 1). The radiation wavelength can be precisely tuned within the ranges mentioned above; the relative linewidth of the radiation spectrum is ~0.2–1%. The laser radiation is linearly polarized and completely spatially coherent. The laser beam intensity profile has a Gaussian shape. For brevity below we refer to NovoFEL radiation as THz radiation, independently of the FEL used/discussed.

3.3. THz multimodal waveguide and optical scheme of the setup

Optical elements used in the cryostat (quartz windows) and EPR resonator (sapphire or BGO dielectric insert) are not transparent in certain ranges of far-IR-mid-IR radiation. Therefore, the most straightforward way to feed radiation directly to the sample in the EPR resonator is to use a sample holder which also plays a role of hollow waveguide for THz radiation. Instead of standard sample holder (a rod of ~60 cm length and 8 mm in diameter), a glass tube of the same outer diameter and similar length is used. The inner diameter of the tube is 5 mm. The sample access size of the EPR dielectric resonator is limited by the inner diameter of corresponding dielectric insert: 5 mm for standard sapphire insert and 4 mm for BGO insert used in this work. To fit to this size, the glass tube has a narrowing to 3.6 mm or less (outer diameter) at one of its ends. Tollens' reagent was used to apply a silver mirror at the inner surface of the tube making it reflective for NovoFEL radiation. The only part of inner surface of the tube which was free of the silver mirror is the narrowed end of the tube positioned in the EPR resonator (Fig. 3a). THz waveguide has been characterized by transmittance and polarization-retaining parameters at two wavenumbers (Table 2).

Relatively low transmission coefficient of the waveguide used is mainly caused by conversion losses of the Gaussian beam to main waveguide modes and reflection of the light at the narrowed end of the waveguide. Polarization preservation coefficient of the waveguide is quite high and therefore polarization-sensitive experiments can be performed.

The size of the THz beam coming out of the nitrogen-filled beamline of NovoFEL (Table 1) was adjusted to the cross section of THz waveguide using optical system (Fig. 3b) of two off-axis

Table 2
Transmission and polarization-retaining coefficients of the THz waveguide measured at 52 cm^{-1} and 77 cm^{-1}.

Wavenumber, cm^{-1}	77	52
Transmittance, (P_{in}/P_{out})	0.11	0.21
Polarization preservation, $(P_{max} - P_{min})/P_{max}$	0.44	0.34

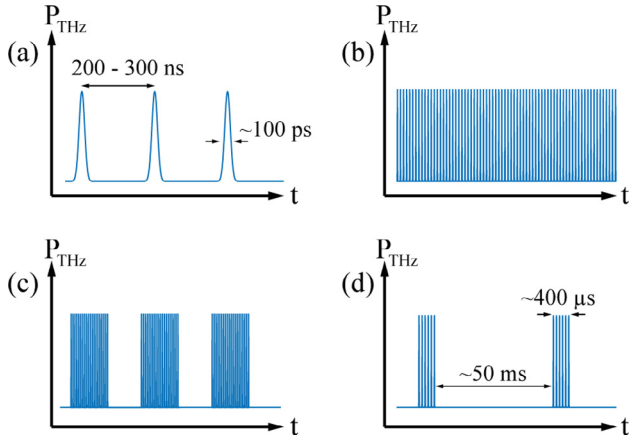

Fig. 4. THz radiation time profiles proposed for experiments at NovoFEL X-band EPR station. (a) Individual THz pulses for the study of fast relaxing processes; (b) quasi-continuous THz radiation for CW EPR On/Off experiments; (c) power-modulated quasi-continuous THz radiation for lock-in detection at the modulation frequency; (d) THz pulse packets for TR EPR experiments.

parabolic mirrors. The mirrors compress the THz beam by a factor of ~15. Optical system is equipped with mechanical shutter and diaphragms to attenuate the incident radiation; it also has THz power probe and tuning mechanism to align the THz beam and waveguide. In the THz pathway between the optical system and waveguide entrance, the beam-modulating devices can be installed (discussed in the next section). The sample under the study is placed at the bottom of the sample holder (THz waveguide) which is covered with polyethylene film cap transparent for THz radiation (Fig. 3a). Then the waveguide with the sample is inserted into the EPR resonator (Fig. 3c). The THz power is measured at the output of THz power probe by Gentec-EO UP19K-15S-VR detector preliminary calibrated for THz frequencies used in experiments.

3.4. Types of proposed experiments

X-band EPR setup at NovoFEL grants the unique opportunities for selective excitation of spin, vibrational or low-lying electronic levels of the system under study (see Section 2); the response to this excitation is simultaneously recorded by X-band EPR. Here we consider the experimental approaches attainable using this setup in general perspective.

Taking into account quasi-stationary character of NovoFEL radiation, several types of experiments using CW and TR EPR modes can be proposed. In this work we discuss prospectively five of them (i-v) and demonstrate experimentally last three in test experiments:

(i) As was mentioned above, THz radiation of NovoFEL consists of continuous train of THz pulses. The duration of individual pulse and spacing between them vary from 10 to 100 ps and from 133 to 267 ns, respectively, depending on the FEL used (Table 1). In the case of fast-relaxing processes the pulsed structure of radiation (Fig. 4a) causes the modulated response of the system under study, and the THz pulse repetition frequency can be used for lock-in detection of the modulated signal.

(ii) The kinetics induced by single THz pulse can as well be recorded in TR EPR experiments with high repetition rate. This experiment also requires fast relaxation times to let spin system fully revert to original state between the THz pulses. In addition, critically coupled EPR resonators with low Q-value have to be used in this approach. As a result, such high frequency lock-in detection and TR experiments are hardly feasible without modification of EPR probehead and even thus can be applied to some limited objects only.

(iii) The EPR sample properties can be changed (ir)reversibly under continuous exposure to THz light (Fig. 4b). Such influence can be studied with EPR spectroscopy by comparing CW EPR spectra measured with THz irradiation on/off (shown in Section 4.1).

(iv) Power modulation of the THz light (Fig. 4c) can be used to make the THz induced changes more evident. This can be done during recording of CW EPR spectrum (shown in Section 4.1); alternatively, the lock-in detection at the power modulation frequency can be employed.

(v) The use of an optical chopper with a small duty cycle (0.5% in this work, see Fig. S5 in Supplementary Material) allows the formation of short (800–400 µs) pulse packets at the repetition rate of 10–20 Hz (Fig. 4d). Optical chopper also significantly reduces the average power applied to the sample and thus prevents its overheating. Processes induced by such THz pulse packets can be studied by EPR in TR mode (shown in Section 4.3).

3.5. Choice of samples and preparation

Two complexes have been used as test samples: mononuclear cobalt(II)-based $NBu_4[CoPiv_3]$ (where NBu_4 is tetrabutylammonium ion and Piv is pivalate) and polymer chain copper(II)-based $Cu(hfac)_2L^{Pr}$ (where $Cu(hfac)_2$ is copper(II) bis-hexafluoroacetylacetonate and L^{Pr} is pyrazolyl-substituted nitronyl nitroxide radical) referred to as **I** and **II**, respectively. The synthesis and structure of **I** were reported earlier [66]. The geometry of coordination environment of the central Co(II) ion (S = 3/2) in **I** is close to a trigonal prism (Fig. 5a), which is favorable for single-ion magnet (SIM) behavior with high Orbach relaxation barrier [67,68]. Although the magnetic properties of **I** were not yet studied, we use this complex here as a test system whose EPR and far-IR properties are similar to the other Co(II)-based SIMs. Thus, in the following experiments we assume that the high-power THz radiation excites the vibrational modes of **I** rather than transitions between its spin levels. To prepare the sample, 11 mg of **I** was finely ground, mixed with 60 mg of powdered polyethylene and compressed into a pellet of 13 mm diameter. Far-IR spectra of this pellet were measured (Fig. S6 in Supplementary Material) and used to select the proper wavelength of THz radiation. A piece of pellet was placed in the THz waveguide for EPR experiments.

Structural, magnetic [69], EPR [51] and optical (including far- and mid-IR) [70,71] properties of compound **II** (Fig. 5b) were studied earlier. Contrary to sample **I**, the spin relaxation times of **II** are less temperature dependent and EPR signals can be observed in a wide temperature range as is usually the case for copper(II) complexes. Single crystal of **II** of $\sim 0.2 \times 0.2 \times 0.5$ mm^3 size was used in experiments.

Both test compounds belong to magnetically concentrated systems with no spin-echo signals detectable even at low (5 K) temperatures. Although spin-lattice (T_1) relaxation time in these systems is not known, we assume it to be short enough, so that the populations of the spin levels follow the changing temperature of the sample on a sub-millisecond timescale.

Sample **I** was irradiated at $k = 86$ cm^{-1} where its absorbance was less than 0.4 (Fig. S6 in Supplementary Material) implying

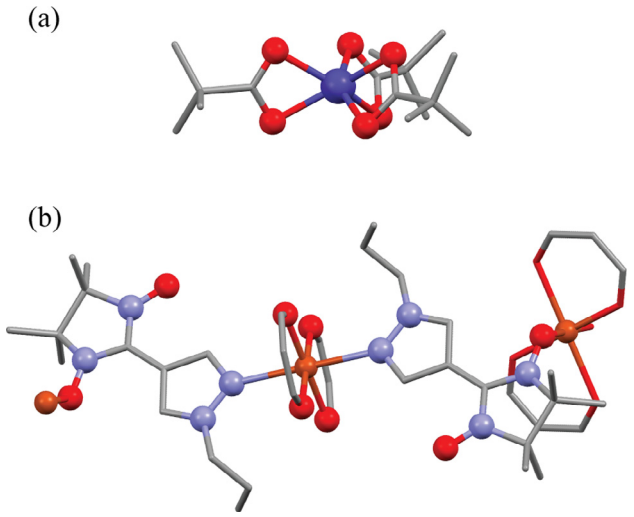

Fig. 5. Chemical structures of the compounds used as test samples: (a) NBu_4[-$CoPiv_3$] and (b) $Cu(hfac)_2L^{Pr}$. Co(II) ion: deep blue, O:red, N: light blue, C: gray, Cu(II) ion: orange. NBu_4, H atoms and CF_3 groups are omitted for clarity. (For interpretation of the references to colour in this figure legend, the reader is referred to the web version of this article.)

almost homogeneous irradiation of the sample volume. Due to the small size of single crystal **II**, its absorbance at the excitation wavenumber ($k = 76\ cm^{-1}$) was unknown. However, sample **II** was also assumed (semi-)transparent, since the far-IR spectrum of $Cu(hfac)_2L^{Pr}$ has no intense absorption bands in this spectral range [70]. In all the experiments performed the pressure of He cooling gas in the EPR cryostat was equal to atmospheric one.

4. Thermal dynamics of the EPR samples

Experimental setup described in this work allows performing time-resolved experiments with THz light excitation and X-band EPR detection, in this way revealing the influence (direct or indirect) of high-power THz radiation on the spin system. Independently of the type of dipole transitions (magnetic or electric) targeted by THz light, the interaction of high-power THz radiation with the sample leads to (at least) partial absorption of radiation resulting in the heating of the sample. Therefore, the control of the sample temperature in such experiments is of high importance for the subsequent data interpretation: as will be shown later, the sample heating results in intense transient EPR signals. T-jump transient EPR applied in this work allowed us to study thermal dynamics of typical EPR samples in detail, being important for future experiments with NovoFEL, because it is absolutely necessary to distinguish between such heating/cooling effects and non-equilibrium spin dynamics induced by THz light pumping of spin system.

The power level of continuous THz radiation required for T-jump EPR observation strongly depends on a number of sample properties and experimental conditions. These include an absorbance of studied sample at THz range, sample size/shape, the location of the sample at the bottom of THz waveguide (irradiation efficiency), temperature of experiment, THz waveguide losses, alignment of THz waveguide with the beam, etc. In the experiments described below the power of quasi-stationary THz radiation did not exceed several watts and was decreased/modulated upon experimental requirements. T-jump transient EPR signals could be observed at sub-watt THz power level.

4.1. CW EPR spectra of *I* irradiated continuously by THz light

Fig. 6a shows the temperature dependence of the EPR spectrum of **I**. Q-value of the EPR resonator used is almost constant at temperatures <40 K [61]; therefore the observed spectral changes reflect the property of the sample (its temperature, relaxation times, etc.), but not the detection scheme. The EPR signal almost disappears at 30 K, and further temperature increase does not lead to significant spectral changes. Irradiation of the sample with THz light leads to significant decrease of the signal intensity and broadening of the EPR lines (Fig. 6b, red). The changes observed are completely reversible: when THz light is switched off the CW EPR spectrum of **I** coincides with initial one. Shuttering of the THz light during the CW EPR spectrum measurement results in fast (on the timescale of CW EPR) switching of the sample spectrum between these two limits (Fig. 6b, blue). We assign this effect to a heating of the EPR sample by THz light, because: (a) CW EPR spectrum at 30 K (THz off) is similar to CW EPR spectrum at 5 K with THz on; (b) the THz-induced spectral changes are completely reversible; (c) THz quanta used have low energy (the photo-induced processes are improbable); (d) the observed effect is reproducible using another THz frequencies. Comparison of Fig. 6a and b leads to conclusion that the THz light heats up the EPR sample from 5 K to T ≥ 30 K in the described experiment. Fast timescale of the observed changes upon switching the THz light on/off indicates that: (i) only the sample is heated by THz light, but not the part of EPR resonator or cryostat, and (ii) time-resolved EPR can be applied to study these processes in more detail.

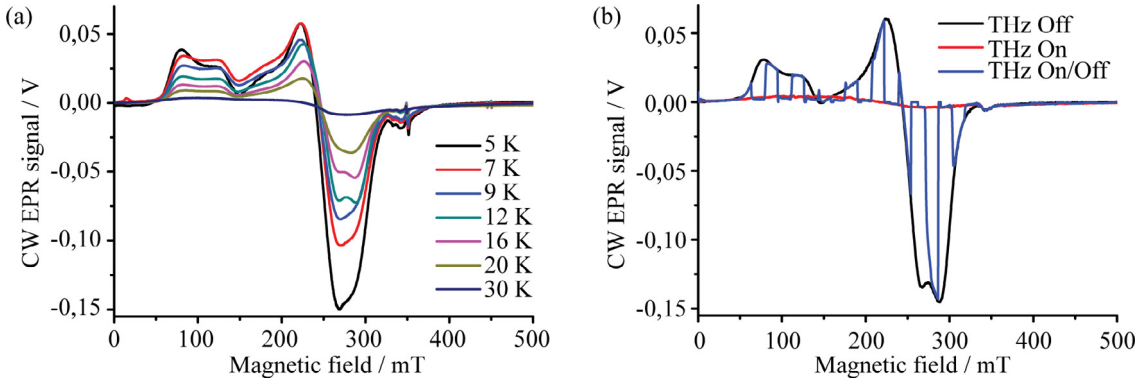

Fig. 6. (a) Temperature dependence of the CW EPR spectrum of **I**. Temperatures are indicated on the right. (b) CW EPR spectrum of **I** measured at 5 K without (black) and under (red) THz radiation. Blue spectrum was recorded by shuttering the THz light with 0.5 Hz frequency. EPR parameters of the CW spectra: mw frequency = 9.81 GHz, mw power (P_{mw}) = 0.2 mW, modulation frequency = 100 kHz, lock-in time constant = 30 ms. (For interpretation of the references to colour in this figure legend, the reader is referred to the web version of this article.)

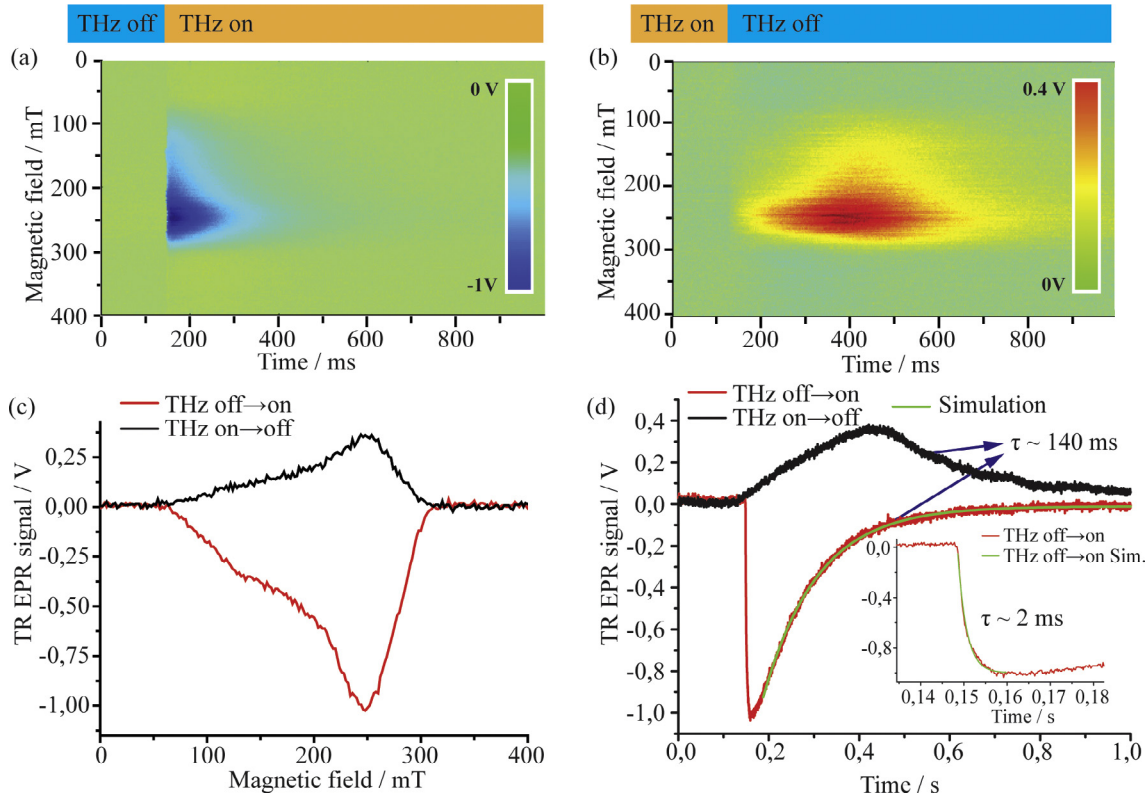

Fig. 7. (a) TR EPR data of **I** triggered by switching on the THz light, (b) TR EPR data of **I** triggered by switching off the THz light, (c) TR EPR spectra taken at 160 ms (red) and 420 ms (black), and (d) TR EPR kinetics taken at global maximum of the spectrum (247 mT for both). τ is the decrement in monoexponential decay function exp(−t/τ) used for kinetic simulation. Blue-yellow bars above the TR data indicate the time profile of THz power applied to the sample. The base temperature was 5 K. TR EPR settings: mw frequency = 9.81 GHz, P_{mw} = 0.2 μW, magnetic field step = 2 mT, number of scan averages = 1. (For interpretation of the references to colour in this figure legend, the reader is referred to the web version of this article.)

*4.2. T-jump TR EPR of **I** induced by low-frequency (~0.5 Hz) THz light shuttering*

Prior to considering time-resolved (TR) EPR spectroscopy of **I**, we would like to briefly mention the differences of measurement approaches in TR and CW modes. CW EPR employs external magnetic field modulation and subsequent lock-in detection of the signal, which results in derivative-like shape of the spectrum. TR EPR does not employ field modulation, but records mw absorption changes upon external influence on the spin system (e.g. laser pulse). Because of that TR EPR spectrum corresponds to the zero-harmonic (not derivative-like) line shape. In many situations, before applying light the EPR spectrum is simply absent. However, if this is not the case, but external stimulus switches the spin system between states having two different EPR spectra, the sign and shape of the resulting TR EPR spectrum will depend on this difference [54,56]. Summarizing all these points, in our case the TR EPR spectrum of **I** recorded upon shuttering of THz light on/off should correspond to the difference of the two (THz on/off) zero-harmonic EPR spectra (i.e. first integrals of CW EPR spectra) (see Fig. S7a in Supplementary Material).

In this type of experiment, we trigger the oscilloscope by the THz light mechanical shutter with repetition rate of ~0.5 Hz and record transient processes induced by the THz light. The duty cycle of THz radiation equals to ~50% meaning that sample is repeatedly exposed to THz light for ~1 s and then relaxes during ~1 s. Such low repetition rate was used to ensure that the stationary temperature is achieved before each triggering (THz off → on or THz on → off). The observed transient signals are filtered by ~1.1 Hz high-pass filter of the EPR detection scheme. Both processes THz off → on (Fig. 7a) and THz on → off (Fig. 7b) can be recorded at the base temperature of 5 K. The 2D TR EPR data (intensity vs. time and magnetic field), TR EPR spectra taken at the maximum of kinetics, and TR EPR kinetics taken at the global maximum of the spectrum are shown in Fig. 7. TR EPR kinetics and spectra have opposite signs for THz light off → on and on → off processes. As expected, the shape of TR EPR spectra (Fig. 7c) looks quite similar to the mw absorption difference of **I** measured in CW mode at two limits: THz off and THz on (Fig. S7b in Supplementary Materials). This confirms that the processes observed in TR mode and the spectral changes recorded in CW mode have the same origin and are caused by thermal influence of THz light. Although TR detection is less sensitive compared to CW mode, it accesses the time profile of the EPR signal change upon external stimulus and provides insights into the characteristic heating/cooling times of the EPR sample. The rise of the signal upon THz off → on (heating) occurs with τ ~ 2 ms and originates from the sample (here and below we use the same letter τ to characterize thermal relaxation; it is obtained by fitting the experimental curve with monoexponential function exp(−t/τ)). The subsequent decay kinetics occurs with τ ~ 140 ms (Fig. 7d, red) and is determined by the lower frequency limit (~1.1 Hz) of the EPR detection scheme (Fig. S1 in Supplementary Materials). The manifestation of THz on → off process (cooling) is different: first the signal gradually rises (originates from the sample) with the time constant of ~100–200 ms, and then the suppression of this signal by the EPR detection scheme (with τ ~ 140 ms) overcomes the rising trend (Fig. 7d, black).

CW EPR with THz light on/off and TR EPR with low-frequency (<1 Hz) THz light shuttering allowed conclusions on the amplitude and timescales of the induced temperature jumps and thus

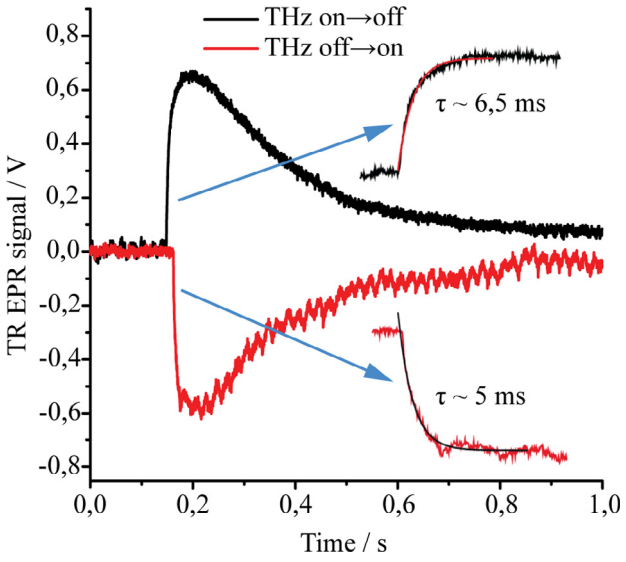

Fig. 8. Kinetics of the TR EPR spectrum of **I** triggered by switching on (red) and off (black) the THz light and recorded at magnetic field with maximum signal intensity (247 mT for both). The base temperature was 5 K. EPR parameters of the TR spectra: mw frequency = 9.81 GHz, P_{mw} = 20 μW, number of scan averages = 1. (For interpretation of the references to colour in this figure legend, the reader is referred to the web version of this article.)

can be used to the temperature jump adjustment/limitation. For the THz power used in the above experiments, CW EPR revealed the heating of the sample from 5 to ≥30 K. In turn, TR EPR data showed that such temperature jump ($\Delta T \geq 25$ K) results in TR signal amplitude of ~1 V at P_{mw} = 0.2 μW. To control the sample temperature jump amplitude in TR EPR experiments with THz pulse packet excitation (see Section 4.3) we should "calibrate" the EPR response of the sample to its temperature changes. Assume we need a temperature jump of $\Delta T \leq 1$ K at base temperature of 5 K. To estimate the TR EPR response we can do the following: (i) run CW EPR experiment with THz light on/off and adjust the THz power level so that the spectrum taken at 5 K with THz on corresponds to the spectrum taken within the temperature range of 5–6 K with THz off (Fig. S8 in Supplementary Material); (ii) measure the corresponding maximum amplitude of the TR EPR kinetics recorded with low-frequency (<1 Hz) THz light shuttering (Fig. 8). According to Fig. 8, the sample temperature jump of $\Delta T \leq 1$ K results in THz-induced TR EPR signal with the amplitude of ~0.6 V at P_{mw} = 20 μW. Note that for such a small temperature jump ($\Delta T \leq 1$ K) the cooling process and the heating one occur with almost the same characteristic time (~5–7 ms), contrary to the situation for $\Delta T >$ 25 K (Fig. 7d). The subsequent decay of the signal originates from the EPR detection scheme (Fig. S1 in Supplementary Materials).

Due to the strong change of the spin level population upon heating of the sample at He temperatures the lock-in detection can also be applied to observe the EPR lines of temperature modulated sample [72]. This technique is particularly useful for recording the broad lines, because the sensitivity of widely employed external magnetic field modulation approach decreases upon an increase of the EPR line width. Temperature modulated technique effectively works with the modulation frequency up to 30 Hz, being limited by the thermal relaxation time of the sample. Note, when the light source with high-energy quanta is used (such as tungsten, Mercury lamps or UV–Vis laser systems) a great care must be taken to sort out the photo-induced signals from the temperature-modulated ones.

4.3. T-jump TR EPR of **I** with $\Delta T < 1$ K and $\Delta T \sim 5$–7 K

The use of short THz pulses (Fig. 4d) benefits from the higher peak intensities of THz light tolerating the moderate sample heating. As was mentioned above, NovoFEL emits high-power quasi-stationary THz radiation which cannot be focused on the sample without its excessive temperature increase. Implementation of the optical chopper wheel of 0.5% duty cycle rotating with ~20 Hz frequency reduces the average THz power significantly and forms the high-power THz pulse packets of 300–400 μs length. In the absence of direct THz pumping of the spin system (the case assumed in this work) the TR EPR signals induced by THz pulse packets are caused by sample temperature jump and trace both heating and cooling dynamics of the sample.

T-jump EPR spectra of **I** observed at the base temperature of 5 K with the sample temperature jump $\Delta T < 1$ K (Fig. 9a) and ΔT ~5–7 K (Fig. 9b) are shown (in order to estimate the amplitude of temperature jump a procedure described in Section 4.2 was performed). Although the magnetic field dependence of these spectra is identical, their time dependence (Fig. 9c, d) is clearly different. While the signal drop time (temperature rise time) is the same in both cases (~400 μs, THz pulse packet length), the subsequent thermal relaxation time τ is ~2.0 ms for $\Delta T < 1$ K and ca. two times longer τ = 4.3 ms for ΔT ~5–7 K. The observed slow down of the thermal relaxation upon the increase of the temperature jump amplitude shows a clear trend converging to the very slow (τ ~100–200 ms) thermal relaxation at $\Delta T \geq 25$ K shown in Section 4.2.

This observation might be explained by the different thermal relaxation rate of the sample at different temperatures, and traces back to the temperature dependence of thermal capacity of the sample. To investigate this effect in more detail, T-jump TR EPR spectra should be measured at different base temperatures. Paramagnetic species with S = 1/2 are superior for this task compared to high-spin S = 3/2 system due to their simpler temperature behaviors.

4.4. T-jump TR EPR spectra of **II** measured at different base temperatures

At temperatures below 90 K the EPR properties of **II** can be modeled by two independent S = 1/2 spin systems. First one belongs to weakly-interacting copper(II) ion with the hyperfine structure ($I_{Cu^{63/65}}$ = 3/2) resolved. Second one belongs to exchange-coupled nitroxide-copper(II)-nitroxide cluster with strong antiferromagnetic copper(II)-nitroxide exchange interaction. These systems have different g-tensors and can be spectrally separated when single crystal is studied. Fig. S9 in Supplementary Material shows chemical structure of **II** with its paramagnetic species highlighted (Fig. S9a) and assigns these species to the CW EPR signals observed in the experiments (Fig. S9c). T-jump TR EPR data of **II** measured at 5 K (Fig. S9b) and the corresponding spectrum (Fig. S9d) are also shown in Supplementary Material. Time dependence of T-jump EPR signals was found the same for all the peaks (four peaks of weakly-interacting copper(II) ion and one peak of exchange-coupled nitroxide-copper(II)-nitroxide cluster). The intensity of copper(II)-nitroxide line is the highest (Fig. S9c), therefore this EPR signal was traced at different temperatures.

T-jump TR EPR signals of **II** measured at the magnetic field of 351.5 mT (EPR line of nitroxide-copper(II)-nitroxide cluster) and different base temperatures 5–20 K are shown in Fig. 10a; THz power applied in these experiments was constant. The same spectra, but normalized, are shown in Fig. 10b. As one can see, both the signal amplitude and the thermal relaxation time of T-jump-induced EPR signal depend on temperature. Temperature

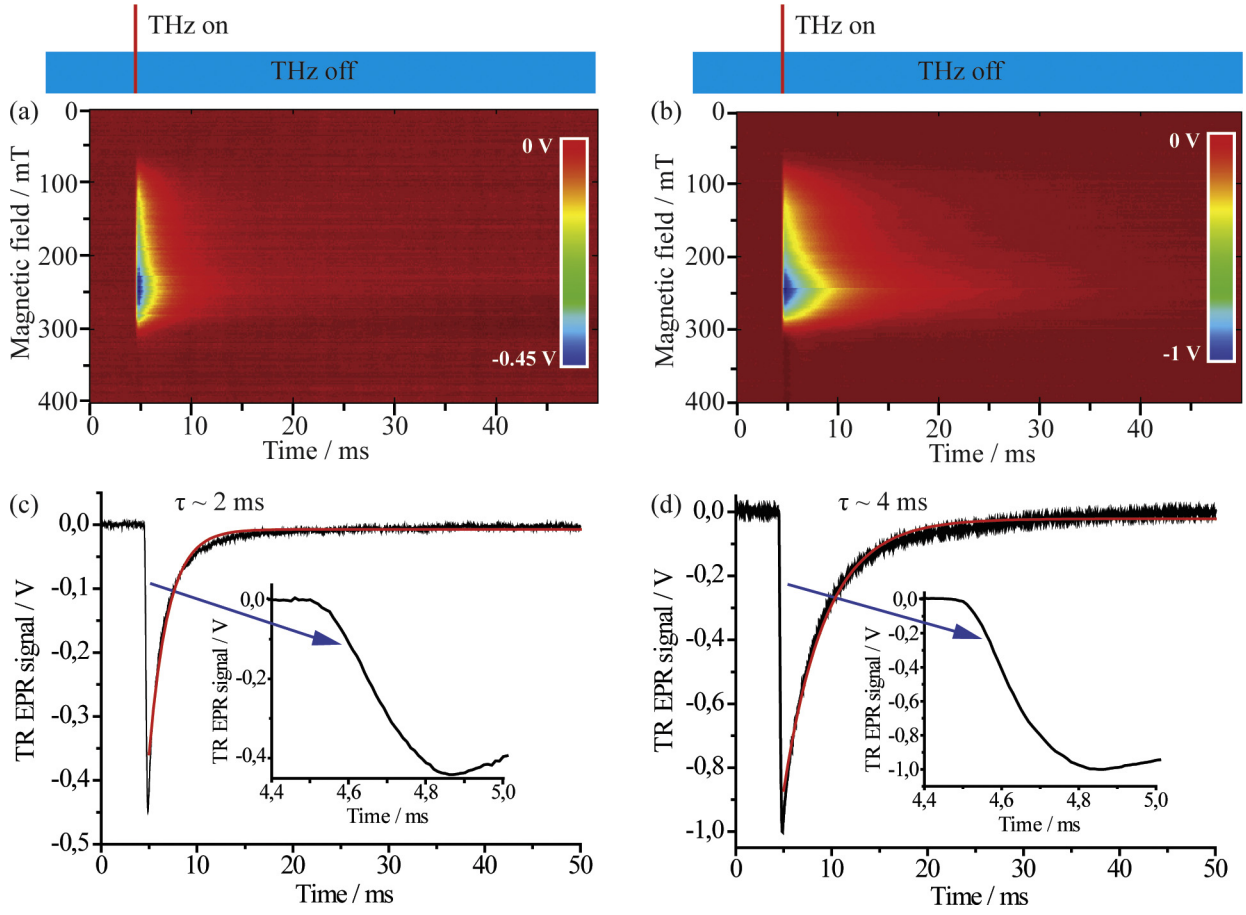

Fig. 9. (a) T-jump TR EPR data of **I** induced by ~400 μs THz pulses. EPR sample temperature jump ΔT is <1 K. (b) T-jump TR EPR data of **I** induced by ~400 μs THz pulses. EPR sample temperature jump ΔT is ~5–7 K. (c, d) Kinetic cross-section of corresponding TR EPR data taking at the magnetic field with maximum signal intensity (247 mT for both). Blue-red bars above the TR data indicate the time profile of THz power applied to the sample. The base temperature was 5 K. EPR parameters of the TR spectra: mw frequency = 9.81 GHz, P_{mw} = 20 μW (a) and 2 μW (b), magnetic field step = 2 mT, number of scan averages = 20. (For interpretation of the references to colour in this figure legend, the reader is referred to the web version of this article.)

dependence of the T-jump EPR amplitude is shown in Fig. 10c. Starting from more than 2500 mV at 5 K, the signal amplitude drops down to ~30 mV at 20 K (see Fig. 10c inset). Fit of this curve by monoexponential decay function $\exp(-T/T_0)$ with the decrement T_0 yields $T_0 \sim 2.4$ K. Temperature dependence of the thermal relaxation time constant is much weaker; nevertheless it changes from $\tau \sim 7$ ms at 5 K to almost 30 ms at 18 K.

4.5. Discussion of the thermal dynamics observed

Thermal dynamics of EPR sample induced by high-power radiation depends on a number of factors (Section 4). In this regard, our consideration below will be rather qualitative than quantitative. Nevertheless, we expect that such parameter as thermal relaxation time discussed below should be similar for various EPR samples of similar size.

The time required for thermal equilibration strongly depends on the temperature jump amplitude induced by applied radiation (the base temperature of 5 K is assumed). Thus, when the temperature jump is limited by <1 K, the steady state temperature is approached with 5–6 ms time constant (Fig. 8). Moreover, this value should be considered as the upper limit, since it includes the time required to cut the THz beam by mechanical shutter. TR EPR experiments performed at this temperature jump show the thermal relaxation time constant of 2 ms and this value can be considered as the lower limit for EPR sample at 5 K and 1 Atm of He pressure (at least, in our experiments we did not observe faster cooling processes so far). The increase of the temperature jump amplitude leads to a rapid slow down of the cooling process, which takes hundreds ms at ΔT > 25 K (Fig. 7d). Such pronounced effect can be explained by strong temperature dependence of the heat capacity (C_p) of the sample. Although this characteristic is unknown for **I**, the data for e.g. Co tungstate $CoWO_4$ is available [73]. Thus, C_p of $CoWO_4$ at 5 K is 10 times smaller than that at 12 K, 100 times smaller than that at 23 K and 10^3 times smaller than that at 90 K. It should be mentioned that the thermal conductivity of He also increases with temperature [74], but less dramatically: at 5 K it is 2 times smaller than that at 12 K and 10 times smaller than that at 170 K. Very low C_p at He temperatures favors fast thermal relaxation, while at higher temperatures the relaxation is slowed down significantly due to dramatic increase of the heat capacity of the sample. This also contributes to the deceleration of thermal relaxation observed by T-jump EPR at higher base temperatures (Fig. 10d).

5. Summary

High-power THz laser sources offer unique opportunities to study the (direct/indirect) influence of THz light on the spin system, which is of great interest for such fields as molecular magnetism and spintronics, since the energy splittings of many single-molecule magnets lie in the THz range. The setup described

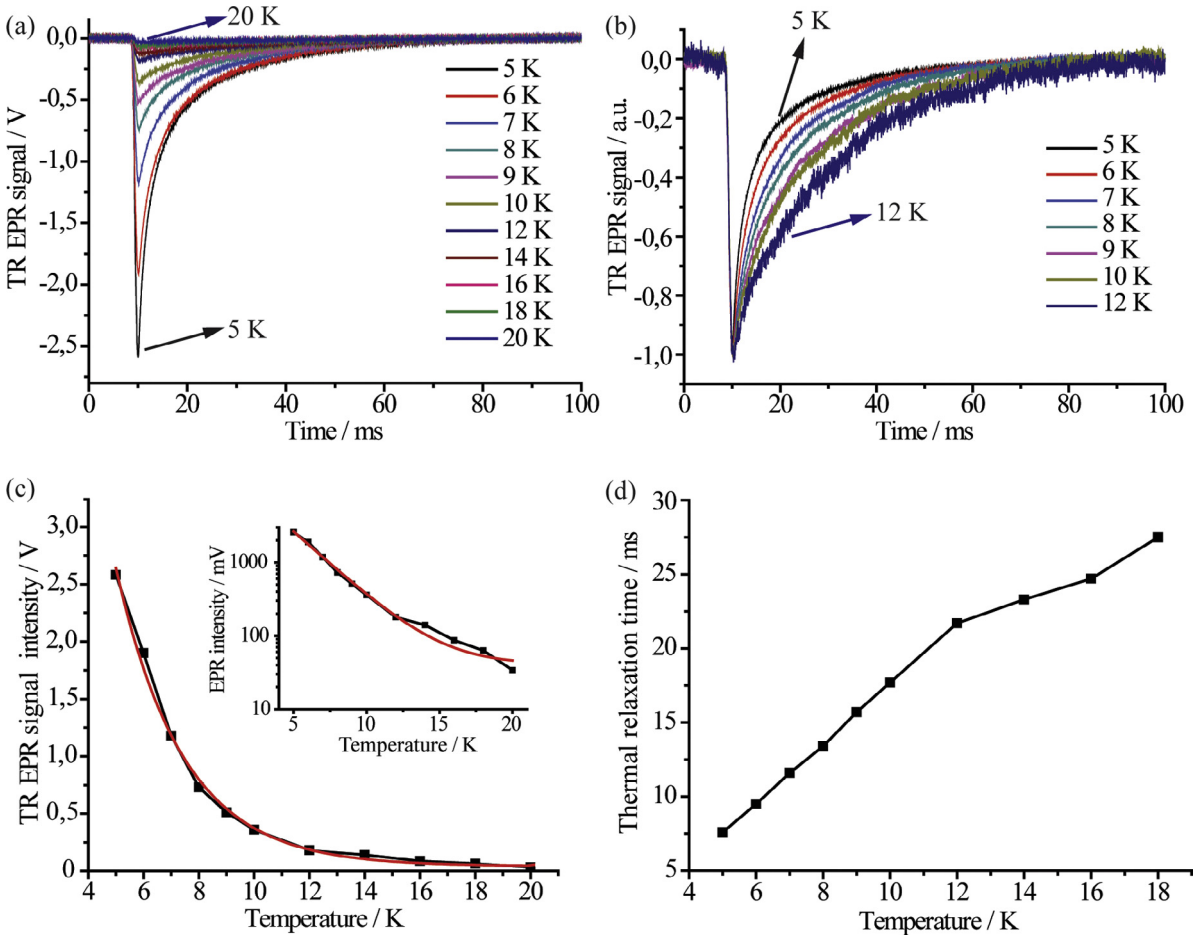

Fig. 10. (a) T-jump TR EPR signals of **II** measured at base temperature 5–20 K. (b) Normalized T-jump TR EPR signals of **II** measured at base temperature 5–12 K. (c) Temperature dependence of T-jump EPR signal amplitude. Red curve shows fit by monoexponential decay function $\exp(-T/T_0)$). Inset shows the dependence in logarithmic scale. (d) Temperature dependence of the thermal relaxation time of **II**. The settings of TR EPR experiment: mw frequency = 9.81 GHz, P_{mw} = 20 μW, magnetic field position = 351.5 mT, number of scan averages = 40. (For interpretation of the references to colour in this figure legend, the reader is referred to the web version of this article.)

herein combines X-band (~9 GHz) EPR spectrometer and Novosibirsk Free Electron Laser facility and thus provides means to trace the influence of high-power tunable THz/far-IR/mid-IR laser light on the spin system. The parameters of EPR spectrometer and NovoFEL radiation are described. Attention is paid to the THz excitation scheme, THz waveguide construction and its transmittance and polarization-retaining characteristics. Possible types of experiments utilizing time profile of NovoFEL THz radiation are discussed. In the test experiments performed with high-power THz radiation the concomitant effect consisting in sample heating is considered. It was shown that high-power THz pulses give rise to intense T-jump transient EPR signals which carry the information on thermal dynamics of EPR sample. Thermal relaxation times of EPR samples were found strongly temperature dependent varying from ~2 ms at ~5 K base temperature to >100 ms when the sample is heated up to >30 K. Characterization of the thermal relaxation times performed in this work is important for distinguishing between T-jump transient EPR signals and THz induced non-equilibrium spin dynamics in the future THz-pump X-band EPR-probe experiments.

Acknowledgments

This work was supported by Russian Science Foundation (No. 17-13-01412). The access to the THz radiation facility, NovoFEL, is provided via the centre of collective usage (supported by The Ministry of Education and Science of The Russian Federation, project RFMEFI62117X0012). S.L.V. is grateful to Mikhail Ivanov for his help with TR EPR data analysis.

Appendix A. Supplementary material

Supplementary data associated with this article can be found, in the online version, at https://doi.org/10.1016/j.jmr.2018.01.009.

References

[1] X.C. Zhang, A. Shkurinov, Y. Zhang, Extreme terahertz science, Nat. Photon. 11 (2017) 16–18.
[2] X. Yin, B.W.-H. Ng, D. Abbott, Terahertz sources and detectors, in: Terahertz Imaging for Biomedical Applications: Pattern Recognition and Tomographic Reconstruction, Springer New York, New York, NY, 2012, pp. 9–26.
[3] R.A. Lewis, A review of terahertz sources, J. Phys. D Appl. Phys. 47 (2014) 374001.
[4] S.H. Gold, G.S. Nusinovich, Review of high-power microwave source research, Rev. Sci. Instrum. 68 (1997) 3945–3974.
[5] P. Tan, J. Huang, K.F. Liu, Y.Q. Xiong, M.W. Fan, Terahertz radiation sources based on free electron lasers and their applications, Sci. China-Inf. Sci. 55 (2012) 1–15.
[6] A. Schnegg, Very-high-frequency EPR, eMagRes 6 (2017) 115–131.
[7] H.Y. Bai, J.G. Kynoch, S.T. Hannahs, Upgrade of the NHMFL cryogenic system and the index heating test results on the 45-T hybrid, IEEE Trans. Appl. Supercond. 26 (2016).
[8] T.A. Painter, J.R. Miller, L.T. Summers, A. Bonitooliva, A.L. Devernoe, G.M. Ciancetta, M.J. King, J. Bascunan, G. Rutman, R.M. Schaedler, H. Boghosian, A. Shapiro, Progress in the manufacture of the cable-in-conduit Nb3Sn outsert coils for the 45-tesla hybrid magnet, IEEE Trans. Magn. 30 (1994) 2204–2207.

[9] Y.M. Eyssa, M.D. Bird, B.J. Gao, H.J. SchneiderMuntau, Design and analysis of a 25T resistive NMR magnet, IEEE Trans. Magn. 32 (1996) 2546–2549.
[10] P.J. Bratt, E. Ringus, A. Hassan, H. Van Tol, A.L. Maniero, L.C. Brunel, M. Rohrer, C. Bubenzer-Hange, H. Scheer, A. Angerhofer, EPR on biological samples beyond the limits of superconducting magnets - The primary donor cation of purple bacterial photosynthesis, J. Phys. Chem. B 103 (1999) 10973–10977.
[11] P.J. Bratt, P. Heathcote, A. Hassan, J. van Tol, L.C. Brunel, J. Schrier, A. Angerhofer, EPR at 24 T of the primary donor radical cation from Blastochloris viridis, Chem. Phys. 294 (2003) 277–284.
[12] A.K. Hassan, L.A. Pardi, J. Krzystek, A. Sienkiewicz, P. Goy, M. Rohrer, L.C. Brunel, Ultrawide band multifrequency high-field EMR technique: a methodology for increasing spectroscopic information, J. Magn. Reson. 142 (2000) 300–312.
[13] M. Date, M. Motokawa, A. Seki, S. Kuroda, K. Matsui, H. Nakazato, H. Mollymoto, Submillimeter electron-spin resonance.2. Megagauss magnets and ESR in $CuCl_2 2H_2O$, J. Phys. Soc. Jpn. 39 (1975) 898–904.
[14] B. Wolf, B. Luthi, S. Schmidt, H. Schwenk, M. Sieling, S. Zherlitsyn, I. Kouroudis, New experimental techniques for pulsed magnetic fields - ESR and ultrasonics, Phys. B 294 (2001) 612–617.
[15] H. Ohta, M. Tomoo, S. Okubo, T. Sakurai, M. Fujisawa, T. Tomita, M. Kimata, T. Yamamoto, M. Kawauchi, K. Kindo, Recent developments of high field ESR systems in Kobe, in: N. Kobayashi, N. Toyota, M. Motokawa (Eds.), Yamada Conference Lx on Research in High Magnetic Fields, Iop Publishing Ltd, Bristol, 2006, p. 611.
[16] S. Okubo, H. Ohta, Y. Inagaki, T. Sakurai, High-field ESR systems in Kobe, Phys. B-Condensed Matter 346 (2004) 627–632.
[17] C. Caspers, P.F. da Silva, M. Soundararajan, M.A. Haider, J.P. Ansermet, Field and frequency modulated sub-THz electron spin resonance spectrometer, APL Phonton. 1 (2016).
[18] T.A. Siaw, A. Leavesley, A. Lund, I. Kaminker, S. Han, A versatile and modular quasi optics-based 200 GHz dual dynamic nuclear polarization and electron paramagnetic resonance instrument, J. Magn. Reson. 264 (2016) 131–153.
[19] G. Mathies, H. Blok, J. Disselhorst, P. Gast, H. van der Meer, D.M. Miedema, R.M. Almeida, J.J.G. Moura, W.R. Hagen, E.J.J. Groenen, Continuous-wave EPR at 275 GHz: Application to high-spin Fe3+ systems, J. Magn. Reson. 210 (2011) 126–132.
[20] K.L. Nagy, D. Quintavalle, T. Feher, A. Janossy, Multipurpose high-frequency ESR spectrometer for condensed matter research, Appl. Magn. Reson. 40 (2011) 47–63.
[21] C. Schlegel, M. Dressel, J. van Slageren, Broadband electron spin resonance at 4–40 GHz and magnetic fields up to 10 T, Rev. Sci. Instrum. 81 (2010).
[22] J. van Tol, L.C. Brunel, R.J. Wylde, A quasioptical transient electron spin resonance spectrometer operating at 120 and 240 GHzL, Rev. Sci. Instrum. 76 (2005).
[23] W. Hofbauer, K.A. Earle, C.R. Dunnam, J.K. Moscicki, J.H. Freed, High-power 95 GHz pulsed electron spin resonance spectrometer, Rev. Sci. Instrum. 75 (2004) 1194–1208.
[24] H. Blok, J. Disselhorst, S.B. Orlinskii, J. Schmidt, A continuous-wave and pulsed electron spin resonance spectrometer operating at 275 GHz, J. Magn. Reson. 166 (2004) 92–99.
[25] G. Annino, M. Cassettari, M. Fittipaldi, I. Longo, M. Martinelli, C.A. Massa, L.A. Pardi, High-field, multifrequency EPR spectroscopy using whispering gallery dielectric resonators, J. Magn. Reson. 143 (2000) 88–94.
[26] M.R. Fuchs, T.F. Prisner, K. Mobius, A high-field/high-frequency heterodyne induction-mode electron paramagnetic resonance spectrometer operating at 360 GHz, Rev. Sci. Instrum. 70 (1999) 3681–3683.
[27] G.M. Smith, J.C.G. Lesurf, R.H. Mitchell, P.C. Riedi, Quasi-optical cw mm-wave electron spin resonance spectrometer, Rev. Sci. Instrum. 69 (1998) 3924–3937.
[28] K.A. Earle, D.S. Tipikin, J.H. Freed, Far-infrared electron-paramagnetic-resonance spectrometer utilizing a quasioptical reflection bridge, Rev. Sci. Instrum. 67 (1996) 2502–2513.
[29] E.J. Reijerse, P.J. van Dam, A.A.K. Klaassen, W.R. Hagen, P.J.M. van Bentum, G.M. Smith, Concepts in high-frequency EPR – Applications to bio-inorganic systems, Appl. Magn. Reson. 14 (1998) 153–167.
[30] M. Rohrer, O. Brügmann, B. Kinzer, T.F. Prisner, High-field/high-frequency EPR spectrometer operating in pulsed and continuous-wave mode at 180 GHz, Appl. Magn. Reson. 21 (2001) 257–274.
[31] J. van Slageren, S. Vongtragool, B. Gorshunov, A.A. Mukhin, N. Karl, J. Krzystek, J. Telser, A. Muller, C. Sangregorio, D. Gatteschi, M. Dressel, Frequency-domain magnetic resonance spectroscopy of molecular magnetic materials, Phys. Chem. Chem. Phys. 5 (2003) 3837–3843.
[32] A.A. Konovalov, V.F. Tarasov, Millimeter and submillimeter EPR spectroscopy, Radiophys. Quantum Electron. 50 (2007) 813.
[33] S. Mitsudo, T. Higuchi, K. Kanazawa, T. Idehara, I. Ogawa, M. Chiba, High field ESR measurements using Gyrotron FU series as radiation sources, J. Phys. Soc. Jpn. 72 (2003).
[34] P. Janssen, I. De Wolf, I. Laursen, EPR in LiHoF4 with a far infrared laser, J. Phys. Chem. Solids 46 (1985) 1387–1391.
[35] C. Kutter, H.P. Moll, J. Vantol, H. Zuckermann, J.C. Maan, P. Wyder, Electron-spin echoes at 604 GHz using far-infrared lasers, Phys. Rev. Lett. 74 (1995) 2925–2928.
[36] F. Muller, M.A. Hopkins, N. Coron, M. Grynberg, L.C. Brunel, G. Martinez, A high magnetic-field EPR spectrometer, Rev. Sci. Instrum. 60 (1989) 3681–3684.
[37] H. Ohta, S. Okubo, K. Kawakami, D. Fukuoka, Y. Inagaki, T. Kunimoto, Z. Hiroi, Submillimeter wave ESR system using the pulsed magnetic field and its applications to one dimensional antiferromagnetic system, J. Phys. Soc. Jpn. 72 (2003).
[38] J. Nehrkorn, K. Holldack, R. Bittl, A. Schnegg, Recent progress in synchrotron-based frequency-domain Fourier-transform THz-EPR, J. Magn. Reson. 280 (2017) 10–19.
[39] Y. Rechkemmer, F.D. Breitgoff, M. van der Meer, M. Atanasov, M. Hakl, M. Orlita, P. Neugebauer, F. Neese, B. Sarkar, J. van Slageren, A four-coordinate cobalt(II) single-ion magnet with coercivity and a very high energy barrier, Nat. Commun. 7 (2016).
[40] K. Ray, A. Begum, T. Weyhermüller, S. Piligkos, J. van Slageren, F. Neese, K. Wieghardt, The electronic structure of the isoelectronic, square-planar complexes [FeII(L)2]2- and [CoIII(LBu)2]- (L2- and (LBu)2- = Benzene-1,2-dithiolates): An experimental and density functional theoretical study, J. Am. Chem. Soc. 127 (2005) 4403–4415.
[41] S. Takahashi, L.C. Brunel, D.T. Edwards, J. van Tol, G. Ramian, S. Han, M.S. Sherwin, Pulsed electron paramagnetic resonance spectroscopy powered by a free-electron laser, Nature 489 (2012) 409–413.
[42] S.A. Zvyagin, M. Ozerov, E. Cizmar, D. Kamenskyi, S. Zherlitsyn, T. Herrmannsdorfer, J. Wosnitza, R. Wuensch, W. Seidel, Terahertz-range free-electron laser electron spin resonance spectroscopy: Techniques and applications in high magnetic fields, Rev. Sci. Instrum. 80 (2009).
[43] M. Ozerov, B. Bernath, D. Kamenskyi, B. Redlich, A.F.G. van der Meer, P.C.M. Christianen, H. Engelkamp, J.C. Maan, ATHz spectrometer combining the free electron laser FLARE with 33 T magnetic fields, Appl. Phys. Lett. 110 (2017).
[44] L. Bogani, W. Wernsdorfer, Molecular spintronics using single-molecule magnets, Nat. Mater. 7 (2008) 179.
[45] D.N. Woodruff, R.E.P. Winpenny, R.A. Layfield, Lanthanide single-molecule magnets, Chem. Rev. 113 (2013) 5110–5148.
[46] S. Bertaina, S. Gambarelli, T. Mitra, B. Tsukerblat, A. Müller, B. Barbara, Quantum oscillations in a molecular magnet, Nature 453 (2008) 203.
[47] J. Ferrando-Soria, E. Moreno Pineda, A. Chiesa, A. Fernandez, S.A. Magee, S. Carretta, P. Santini, I.J. Vitorica-Yrezabal, F. Tuna, G.A. Timco, E.J.L. McInnes, R. E.P. Winpenny, A modular design of molecular qubits to implement universal quantum gates, Nat. Commun. 7 (2016) 11377.
[48] K. Petukhov, S. Bahr, W. Wernsdorfer, A.L. Barra, V. Mosser, Magnetization dynamics in the single-molecule magnet Fe_8 under pulsed microwave irradiation, Phys. Rev. B 75 (2007) 064408.
[49] V.V. Novikov, A.A. Pavlov, A.S. Belov, A.V. Vologzhanina, A. Savitsky, Y.Z. Voloshin, Transition ion strikes back: large magnetic susceptibility anisotropy in cobalt(II) clathrochelates, J. Phys. Chem. Lett. 5 (2014) 3799–3803.
[50] K.S. Murray, The Development of Spin-Crossover Research, in: Spin-Crossover Materials, John Wiley & Sons Ltd, 2013, pp. 1–54.
[51] M.V. Fedin, S.L. Veber, E.G. Bagryanskaya, V.I. Ovcharenko, Electron paramagnetic resonance of switchable copper-nitroxide-based molecular magnets: An indispensable tool for intriguing systems, Coord. Chem. Rev. 289 (2015) 341–356.
[52] M.V. Fedin, S.L. Veber, G.V. Romanenko, V.I. Ovcharenko, R.Z. Sagdeev, G. Klihm, E. Reijerse, W. Lubitz, E.G. Bagryanskaya, Dynamic mixing processes in spin triads of "breathing crystals" Cu(hfac)(2)L-R: a multifrequency EPR study at 34, 122 and 244 GHz, Phys. Chem. Chem. Phys. 11 (2009) 6654–6663.
[53] S.L. Veber, M.V. Fedin, K.Y. Maryunina, A. Potapov, D. Goldfarb, E. Reijerse, W. Lubitz, R.Z. Sagdeev, V.I. Ovcharenko, E.G. Bagryanskaya, Temperature-dependent exchange interaction in molecular magnets Cu(hfac)(2)L-R studied by EPR: methodology and interpretations, Inorg. Chem. 50 (2011) 10204–10212.
[54] M.V. Fedin, E.G. Bagryanskaya, H. Matsuoka, S. Yamauchi, S.L. Veber, K.Y. Maryunina, E.V. Tretyakov, V.I. Ovcharenko, R.Z. Sagdeev, W-Band time-resolved electron paramagnetic resonance study of light-induced spin dynamics in copper-nitroxide-based switchable molecular magnets, J. Am. Chem. Soc. 134 (2012) 16319–16326.
[55] M.V. Fedin, K.Y. Maryunina, R.Z. Sagdeev, V.I. Ovcharenko, E.G. Bagryanskaya, Self-decelerating relaxation of the light-induced spin states in molecular magnets Cu(hfac)2LR studied by electron paramagnetic resonance, Inorg. Chem. 51 (2012) 709–717.
[56] I.Y. Barskaya, E.V. Tretyakov, R.Z. Sagdeev, V.I. Ovcharenko, E.G. Bagryanskaya, K.Y. Maryunina, T. Takui, K. Sato, M.V. Fedin, Photoswitching of a thermally unswitchable molecular magnet Cu(hfac)(2)Li-Pr evidenced by steady-state and time-resolved electron paramagnetic resonance, J. Am. Chem. Soc. 136 (2014) 10132–10138.
[57] S.V. Tumanov, S.L. Veber, S.E. Tolstikov, N.A. Artiukhova, G.V. Romanenko, V.I. Ovcharenko, M.V. Fedin, Light-induced spin state switching and relaxation in spin Pairs of copper(II)-nitroxide based molecular magnets, Inorg. Chem. 56 (2017) 11729–11737.
[58] S.L. Veber, M.V. Fedin, K.Y. Maryunina, K.N. Boldyrev, M.A. Sheglov, V.V. Kubarev, O.A. Shevchenko, N.A. Vinokurov, G.N. Kulipanov, R.Z. Sagdeev, V.I. Ovcharenko, E.G. Bagryanskaya, Influence of intense thz radiation on spin state of photoswitchable compound Cu(hfac)(2)L-Pr, J. Phys. Chem. A 117 (2013) 1483–1491.
[59] I.Y. Barskaya, S.L. Veber, E.A. Suturina, P.S. Sherin, K.Y. Maryunina, N.A. Artiukhova, E.V. Tretyakov, R.Z. Sagdeev, V.I. Ovcharenko, N.P. Gritsan, M.V. Fedin, Spin-state-correlated optical properties of copper(II)-nitroxide based molecular magnets, Dalton Trans. 46 (2017) 13108–13117.
[60] R.W. Quine, D.G. Mitchell, G.R. Eaton, A general purpose Q-measuring circuit using pulse ring-down, Concepts Magn. Reson. Part B 39B (2011) 43–46.

[61] M.Y. Ivanov, V.A. Nadolinny, E.G. Bagryanskaya, Y.A. Grishin, M.V. Fedin, S.L. Veber, Bismuth germanate as a perspective material for dielectric resonators in EPR spectroscopy, J. Magn. Reson. 271 (2016) 83–89.
[62] B.A. Knyazev, E.G. Bagryanskaya, E.N. Chesnokov, Y.Y. Choporova, V.V. Gerasimov, Y.V. Getmanov, B.G. Goldenberg, G.N. Kulipanov, A.S. Kozlov, V.V. Kubarev, A.K. Nikitin, V.S. Pavelyev, S.E. Peltek, V.M. Popik, T.V. Salikova, M.A. Scheglov, S.S. Serednyakov, O.A. Shevchenko, A.N. Skrinsky, S.L. Veber, N.A. Vinokurov, Novosibirsk free electron laser as a user facility, Phys. Proc. 84 (2016) 27–34.
[63] E.A. Antokhin, R.R. Akberdin, V.S. Arbuzov, M.A. Bokov, V.P. Bolotin, D.B. Burenkov, A.A. Bushuev, V.F. Veremeenko, N.A. Vinokurov, P.D. Vobly, N.G. Gavrilov, E.I. Gorniker, K.M. Gorchakov, V.N. Grigoryev, B.A. Gudkov, A.V. Davydov, O.I. Deichuli, E.N. Dementyev, B.A. Dovzhenko, A.N. Dubrovin, Y.A. Evtushenko, E.I. Zagorodnikov, N.S. Zaigraeva, E.M. Zakutov, A.I. Erokhin, D.A. Kayran, O.B. Kiselev, B.A. Knyazev, V.R. Kozak, V.V. Kolmogorov, E.I. Kolobanov, A.A. Kondakov, N.L. Kondakova, S.A. Krutikhin, A.M. Kryuchkov, V.V. Kubarev, G.N. Kulipanov, E.A. Kuper, L. Kuptsov, G.Y. Kurkin, E.A. Labutskaya, L.G. Leontyevskaya, V.Y. Loskutov, A.N. Matveenko, L.E. Medvedev, A.S. Medvedko, S.V. Miginsky, L.A. Mironenko, S.V. Motygin, A.D. Oreshkov, V.K. Ovchar, V.N. Osipov, B.Z. Persov, S.P. Petrov, V.M. Petrov, A.M. Pilan, L. Poletaev, A.V. Polyanskiy, V.M. Popik, A.M. Popov, E.A. Rotov, T.V. Salikova, I.K. Sedliarov, P.A. Selivanov, S.S. Serednyakov, A.N. Skrinsky, S.V. Tararyshkin, L.A. Timoshina, A. G. Tribendis, M.A. Kholopov, V.P. Cherepanov, O.A. Shevchenko, A.R. Shteinke, E.I. Shubin, M.A. Scheglov, First lasing at the high-power free electron laser at Siberian Center for Photochemistry Research, Nucl. Instrum. Methods Phys. Res. Sect. A-Accel. Spectrom. Dect. Assoc. Equip. 528 (2004) 15–18.
[64] G.N. Kulipanov, E.G. Bagryanskaya, E.N. Chesnokov, Y.Y. Choporova, V.V. Gerasimov, Y.V. Getmanov, S.L. Kiselev, B.A. Knyazev, V.V. Kubarev, S.E. Peltek, V.M. Popik, T.V. Salikova, M.A. Scheglov, S.S. Seredniakov, O.A. Shevchenko, A. N. Skrinsky, S.L. Veber, N.A. Vinokurov, Novosibirsk free electron laser-facility description and recent experiments, IEEE Trans. Terahertz Sci. Technol. 5 (2015) 798–809.
[65] O.A. Shevchenko, V.S. Arbuzov, N.A. Vinokurov, P.D. Vobly, V.N. Volkov, Y.V. Getmanov, Y.I. Gorbachev, I.V. Davidyuk, O.I. Deychuly, E.N. Dementyev, B.A. Dovzhenko, B.A. Knyazev, E.I. Kolobanov, A.A. Kondakov, V.R. Kozak, E.V. Kozyrev, V.V. Kubarev, G.N. Kulipanov, E.A. Kuper, I.V. Kuptsov, G.Y. Kurkin, S. A. Krutikhin, L.E. Medvedev, S.V. Motygin, V.K. Ovchar, V.N. Osipov, V.M. Petrov, A.M. Pilan, V.M. Popik, V.V. Repkov, T.V. Salikova, I.K. Sedlyarov, S.S. Serednyakov, A.N. Skrinsky, S.V. Tararyshkin, A.G. Tribendis, V.G. Tcheskidov, K.N. Chernov, M.A. Scheglov, The novosibirsk free electron laser – unique source of terahertz and infrared coherent radiation, Phys. Proc. 84 (2016) 13–18.
[66] E. Fursova, G. Romanenko, R. Sagdeev, V. Ovcharenko, Mononuclear Mn(II), Co (II), and Cu(II) pivalates, Polyhedron 81 (2014) 27–31.
[67] V.V. Novikov, A.A. Pavlov, Y.V. Nelyubina, M.-E. Boulon, O.A. Varzatskii, Y.Z. Voloshin, R.E.P. Winpenny, A trigonal prismatic mononuclear cobalt(II) complex showing single-molecule magnet behavior, J. Am. Chem. Soc. 137 (2015) 9792–9795.
[68] A.A. Pavlov, Y.V. Nelyubina, S.V. Kats, L.V. Penkova, N.N. Efimov, A.O. Dmitrienko, A.V. Vologzhanina, A.S. Belov, Y.Z. Voloshin, V.V. Novikov, Polymorphism in a cobalt-based single-ion magnet tuning its barrier to magnetization relaxation, J. Phys. Chem. Lett. 7 (2016) 4111–4116.
[69] V.I. Ovcharenko, K.Y. Maryunina, S.V. Fokin, E.V. Tretyakov, G.V. Romanenko, V. N. Ikorskii, Spin transitions in non-classical systems, Russ. Chem. Bull. 53 (2004) 2406–2427.
[70] S.L. Veber, E.A. Suturina, M.V. Fedin, K.N. Boldyrev, K.Y. Maryunina, R.Z. Sagdeev, V.I. Ovcharenko, N.P. Gritsan, E.G. Bagryanskaya, FTIR study of thermally induced magnetostructural transitions in breathing crystals, Inorg. Chem. 54 (2015) 3446–3455.
[71] I.Y. Barskaya, S.L. Veber, E. Suturina, P.S. Sherin, K.Y. Maryunina, N.A. Artiukhova, E.V. Tretyakov, R.Z. Sagdeev, V.I. Ovcharenko, N.P. Gritsan, M.V. Fedin, Spin-state-correlated optical properties of copper(II)-nitroxide based molecular magnets, Dalton Trans. (2017).
[72] G. Feher, R.A. Isaacson, J.D. McElroy, Observation of EPR lines using temperature modulation, Rev. Sci. Instrum. 40 (1969) 1640–1641.
[73] C.P. Landee, E.F. Westrum, Thermophysical measurements on transition-metal tungstates.2. Heat-capacities of antiferromagnetic nickel and cobalt tungstates, J. Chem. Thermodyn. 8 (1976) 471–491.
[74] N.B. Vargaftik, L.V. Yakush, Temperature dependence of thermal conductivity of helium, J. Eng. Phys. 32 (1977) 530–532.